Numerical Study of Some Unstably Stratified Boundary-Layer Flows over a Valley at Moderate Richardson Number

J. D. CARLSON*

Atmospheric Sciences Program, The Ohio State University, Columbus, Ohio 43210

M. R. FOSTER

Department of Aeronautical and Astronautical Engineering, The Ohio State University, Columbus, Ohio 43210

(Manuscript received 2 June 1984, in final form 17 August 1985)

ABSTRACT

A two-dimensional numerical model is utilized to investigate steady-state, three-dimensional turbulent flow over a valley under unstable thermal stratifications. An eddy viscosity turbulence model is employed, in which the mixing length is a function of distance to the surface, shears of the mean velocity components, and a stability parameter involving Monin–Obukhov length. Three case studies are presented to show the effect of various surface temperature distributions on flow at bulk Richardson numbers in the vicinity of minus one. At such numbers the thermal effects of topography are of the same scale as the dynamic effects. Variables examined for each of the cases include the potential temperature and vorticity over the valley as well as the surface heat flux and shear stress. In addition, the shape and magnitude of the wind speed profiles over the two valley slopes are presented and discussed. Baroclinicity and thermally enhanced turbulent mixing are seen to play important roles. In all three cases the ambient momentum of the geostrophic wind is well-mixed down to the valley surface, preventing any local upslope flows over the windward slope from developing.

1. Introduction

In recent years a large number of analytical and numerical models have been developed for the study of planetary boundary-layer flow under various thermal stratifications. Most of these studies have emphasized flow over flat terrain. However, much of the earth is not flat, with a large portion of the population, industry, and agriculture concentrated within valleys. Over such terrain the atmospheric motions are greatly modified and much less predictable. Accordingly, there has been a growing interest in observing and modeling flow over complex terrain.

Many different types of flows have been observed within valleys, as can be seen in Hewson and Gill (1944), Defant (1951), Lanham (1980), Banta (1981), and Whiteman (1982). When synoptic-scale pressure gradients are weak, local thermal circulations dominate. Such situations are accompanied by nighttime temperature inversions within the valley. Upslope and upvalley winds form during the morning due to solar insolation and may persist until late afternoon, when surface cooling leads to drainage flows in the reverse directions. In addition, with differential solar heating of the valley slopes, a cross-valley wind component may develop during the daytime.

During periods of synoptic influence, once a neutral or convective boundary layer is established throughout the depth of the valley, the ambient momentum of the gradient wind is brought down into the valley through turbulent mixing, effectively masking or preventing any local thermal circulations. Streamlines deform to follow the valley shape. Within the valley, channeling of the synoptic wind toward a direction more nearly parallel to the valley axis often occurs. If the ambient wind is strong enough, flow separation may take place over the windward slope. Thus, for example, while local thermal circulations may occur during the presence of a valley inversion, once that inversion is eroded by convective heating, the upslope wind over the windward valley slope will be replaced by a downslope wind resulting from the momentum transfer of the ambient wind into the valley. Observations by Banta (1981) and Whiteman (1982) indeed show the upslope wind over the windward slope to be a temporary morning phenomenon on days with ambient wind. Their studies show the thermally generated upslope winds to cease by late morning, when the growing convective boundary layer has completely eroded the inversion separating the local thermal circulations from the ambient flow above. At such a time a deep, well-mixed convective boundary layer exists and ambient momentum is transferred into

* Present affiliation: Agricultural Weather Service Office, Department of Entomology, Michigan State University, East Lansing, MI 48824.

the valley, resulting in downslope flow over the windward slope.

While there have been a sizeable number of analytical and numerical studies dealing with valley meteorology under conditions of no ambient wind, the number of studies in the literature concerning synoptic flow over a valley is small. Tang (1976) developed a linear analytical model to investigate two-dimensional flow across a shallow sinusoidal valley under various thermal stratifications. Kao and Liu (1981) obtained an analytical solution for three-dimensional flow over a valley under neutral conditions. Both studies employed a constant eddy viscosity. Taylor (1977a,b) used numerical models to study two- and three-dimensional flows over a Gaussian-shaped valley under neutral stratification. Bell and Thompson (1980) numerically investigated two-dimensional fluid motion across a valley under strong stable stratification. Yamada (1980) developed a numerical model to study three-dimensional time-dependent flow over a three-dimensional Gaussian valley. Both nocturnal stable and daytime convective conditions were simulated.

The present paper describes a numerical model designed to calculate steady-state distributions of wind and temperature for ambient turbulent flow over a valley. Neutral and unstable thermal stratifications can be simulated. In the latter case the assumption of a steady lower boundary layer is based upon observational evidence (Carlson, 1982). Such quasi-steady conditions typically occur on sunny days in mid-afternoon during a one- or two-hour period.

The bulk Richardson number for the present problem indicates the relative importance of thermal effects to dynamic effects. In cases with bulk Richardson numbers near zero, the dynamic interactions of the flow with the valley dominate. In another paper (Carlson and Foster, 1985) four such case studies are presented to show the effects of thermal stratification, geostrophic wind angle, and valley geometry on the flow. The numerical results discussed include the channeling of flow by the valley and the surface distributions of shear stress and heat flux.

In the present paper three case studies with bulk Richardson numbers in the vicinity of minus one (i.e., of order one) are presented. In such flows surface heating becomes important and thermally induced effects occur. In all cases the cross-valley momentum of the ambient wind is well-mixed down to the valley surface, preventing any thermally driven upslope flows over the windward slope from developing. The effect of temperature structure, however, is still seen in that over the windward slope, where baroclinic vorticity production is positive, values of total wind speed are lower than those over the opposite slope. Another manifestation of baroclinicity is the jetlike wind speed maximum over the leeward slope in one of the cases. In addition, it is shown that over a given slope, greater surface heat flux results in increased turbulent mixing, which increases the surface stress (and wind speed shear near the surface). Furthermore, because of the enhanced mixing of momentum resulting from greater surface heating, the wind experiences a smaller degree of directional turning (less channeling).

2. Model equations

For a valley situated at latitude ϕ in the Northern Hemisphere, align the y-axis of a right-handed Cartesian coordinate system with the valley axis. Let the x-axis be in the cross-valley direction and the z-axis in the vertical. The valley dimensions are considered invariant in the y direction (along its axis). In addition, it is assumed that the geostrophic wind and latitude ϕ do not vary over the region of concern. Under such conditions any mathematical solution will be solely a function of x and z. Finally, since the results are not dependent on the orientation of the valley axis, it is taken to be directed northward for convenience in referencing wind direction.

a. Governing equations

The derivation of the five governing equations for the present problem is given in Carlson and Foster (1985) and need not be repeated here. These equations describe the mean turbulent flow and consist of the continuity equation, the x-, y-, and z-momentum equations, and the energy equation.

By defining the streamfunction ψ and the vorticity component ξ about the y-axis,

$$\partial\psi/\partial z = u, \quad \partial\psi/\partial x = -w, \tag{1}$$

$$\xi = \partial u/\partial z - \partial w/\partial x, \tag{2}$$

we can reduce the set of five equations to a set of four, as follows:

$$\nabla^2\psi = \xi, \tag{3}$$

$$D\xi/Dt = -(g/\theta_0)(\partial\theta'/\partial x) + f(\partial v/\partial z) + \nabla^2(K_m\xi) + 2(\partial^2/\partial z^2)(K_m\partial w/\partial x) - 2(\partial^2/\partial x^2)(K_m\partial u/\partial z) - 4(\partial/\partial x)(\partial/\partial z)(K_m\partial w/\partial z), \tag{4}$$

$$Dv/Dt = f(u_g - u) + (\partial/\partial x)(K_m\partial v/\partial x) + (\partial/\partial z)(K_m\partial v/\partial z), \tag{5}$$

$$D\theta'/Dt = (\partial/\partial x)(K_h\partial\theta'/\partial x) + (\partial/\partial z)(K_h\partial\theta'/\partial z), \tag{6}$$

where,

$$D/Dt = \partial/\partial t + u(\partial/\partial x) + w(\partial/\partial z). \tag{7}$$

Here, u, v, and w are the mean flow components in the x, y, and z directions, respectively; u_g is the x-component geostrophic wind; θ' is the potential temperature perturbation from an equilibrium adiabatic atmosphere at θ_0; and K_m and K_h represent the eddy viscosities and diffusivities, respectively. All other variables retain their usual meanings.

b. Turbulence model

In this study, K_m and K_h are assumed to be functions of the mean flow and its gradients, and are written as

$$K_m = 2l_m^2(\mathbf{D}_{ij}:\mathbf{D}_{ij})^{1/2}, \tag{8}$$

$$K_h = 2l_h^2(\mathbf{D}_{ij}:\mathbf{D}_{ij})^{1/2}, \tag{9}$$

where $\mathbf{D}_{ij}$ is the deformation tensor

$$\mathbf{D}_{ij} = 1/2(\partial u_i/\partial x_j + \partial u_j/\partial x_i), \tag{10}$$

and l_m and l_h are the length scales of the energy-containing eddies. Here subscript notation has been used: u_i ($i = 1, 2, 3$) is the mean velocity component in the x_i direction ($x_1 = x$, $x_2 = y$, $x_3 = z$).

In order to model flows under unstable thermal stratifications, the expressions for l_m and l_h must take into account both mechanically and thermally generated turbulence. For a stability parameter we choose the dimensionless height ζ,

$$\zeta = z^*/L, \tag{11}$$

where z^* is the distance to the surface and L the Monin–Obukhov length. The present mixing lengths follow the general form of Blackadar's (1962) model for mixing length under neutral conditions, which allows l to behave as kz^* near the surface (as it should in the log layer) and to approach a constant λ at the upper reaches of the planetary boundary layer. In accordance with well-known scaling relationships in the surface layer (Busch, 1973), the model is modified to include unstable conditions and becomes

$$l_m = \begin{cases} \dfrac{k(z^* + z_0)/\phi_m(\zeta)}{1 + \{k(z^* - \delta^*)/[\lambda\phi_m(\zeta)]\}} & \text{for } z^* > \delta^* \\ k(z^* + z_0)/\phi_m(\zeta) & \text{for } z^* \leqslant \delta^*, \end{cases} \tag{12}$$

$$l_h = \begin{cases} \dfrac{k(z^* + z_0)/[\phi_m(\zeta)\phi_h(\zeta)]^{1/2}}{1 + k(z^* - \delta^*)/[\lambda(\phi_m(\zeta)\phi_h(\zeta))^{1/2}]} & \text{for } z^* > \delta^* \\ k(z^* + z_0)/[\phi_m(\zeta)\phi_h(\zeta)]^{1/2} & \text{for } z^* \leqslant \delta^*. \end{cases} \tag{13}$$

As one can see, the mixing lengths retain their surface layer forms within a height δ^* above the surface. Here k is the von Karman constant and z_0 the surface roughness length. The forms chosen for the nondimensional wind shear ϕ_m and temperature gradient ϕ_h are based on the work of Dyer and Hicks (1970):

$$\phi_m(\zeta) = (1 - 16\zeta)^{-1/4} \quad \text{for} \quad \zeta \leqslant 0, \tag{14}$$

$$\phi_h(\zeta) = (1 - 16\zeta)^{-1/2} \quad \text{for} \quad \zeta \leqslant 0. \tag{15}$$

3. Formulation of the boundary-value problem

a. Description

First, consider the geometric configuration. Figure 1 depicts the cross section of the valley in the x–z plane. As mentioned earlier, the valley dimensions are invariant along its axis.

The region enclosed by the heavily shaded solid-line segments represents the domain of calculation. The left vertical segment is the inflow boundary and the right vertical segment, the outflow boundary. The series of segments at the bottom represent the surface contour S of the valley, whose depth is H. The region of thickness δ lying above S depicts a layer within which temperature and wind profiles are modeled explicitly according to flux-profile relationships in the surface layer (Busch, 1973; Businger, 1973). The upper solid segment at $z = z_t$ is the upper boundary and is at a level dividing

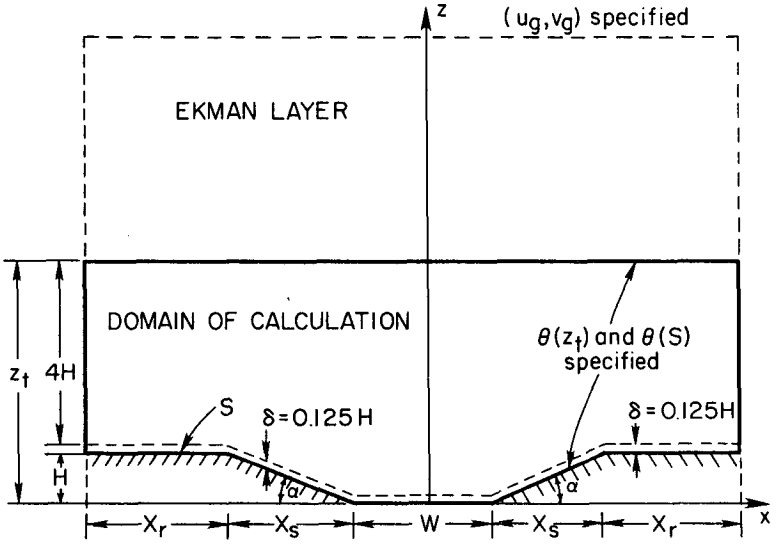

FIG. 1. Geometric configuration for the present problem. The independent parameters are u_g, v_g, $\theta(z_t)$, $\theta(S)$, H, W, and α.

two vertical regions. The lower region, the domain of calculation, is a region of three-dimensional flow and variable K_m and K_h. It is assumed to be well below the capping stable layer during midafternoon and well within the mixed convective layer. The upper region is an assumed Ekman layer of only horizontal flow. The top of this region represents the top of the planetary boundary layer. In the cases studied, $\delta = 15.6$ m, $H = 125$ m, and $z_t = 641$ m.

Any specific problem of interest involves the specification of the geometrical parameters H (valley depth), W (valley floor width), and α (angle of slopes), as well as the following meteorological parameters: 1) the geostrophic wind (u_g, v_g), assumed constant through the boundary layer, 2) the potential temperature θ at $z = z_t$, and 3) the θ distribution along S. The problem is then to seek a steady state solution to Eqs. (3)–(6).

b. *Boundary conditions*

The left inflow boundary presupposes that the flow has been traveling over horizontal terrain and, hence, is uniform in the x direction. At this boundary, then, $\partial\psi/\partial x = 0$ ($w = 0$) and u, v, and θ' are specified from the steady upstream profiles, the solutions for which have been formerly obtained as a separate problem.

The top boundary of the calculation is at $z = z_t$, which we assume to be high enough that w is negligible. If, in addition, barotropic conditions ($\partial\theta'/\partial x = 0$) exist above z_t, then the usual Ekman layer solution is, in fact, an exact solution to (3)–(6) for K_m and K_h constant, provided $\partial u/\partial x$ and $\partial v/\partial x$ are negligible there. A study one of us (JDC) conducted using 1979 data from the Tennessee Valley Authority showed that, for midday situations over a 275 m deep valley in Alabama, the temperature over the ridge and that over the valley were equal by an elevation, on the average, of 950 m. Hence, at a height of $2.5H$ above the ridge, θ' was indeed x-independent. In addition, our numerical solutions show a posteriori the legitimacy of our assumptions: near the top of the domain, u, v, and θ' are nearly x-independent. With such being the case, an Ekman spiral is the only appropriate solution for large distances above the valley. Any lesser, ad hoc boundary condition is incorrect. Finally, even under unstable stratifications, Ekman spirals have been shown to exist both observationally (Zilitinkevich et al., 1967) and theoretically (Yamamoto et al., 1968).

The top boundary, then, is assumed sufficiently high above the valley to allow ψ ($w = 0$) and θ' to be specified constants. Indeed, numerical studies were performed to check the effects of top boundary height on flow; these resulted in the choice of $z_t = 5H + \delta$. The prescribed ψ value is obtained through vertical integration of the upstream u profile. To arrive at the ξ and v boundary conditions, we demand that the computed solution in $z < z_t$ for u, v, $\partial u/\partial z$, $\partial v/\partial z$, and K_m agree with the analytical Ekman solution in $z > z_t$ (here, K_m scales with fU_g). That joining of the two solutions at $z = z_t$ results in expressions for ξ and $\partial v/\partial z$ as a function of x (Carlson and Foster, 1985). These four boundary conditions properly allow for the transport of heat and momentum across the top boundary. Individual features such as thermals or Ekman rolls, while not explicitly resolved, are implicitly included in our turbulence closure scheme, which models time-averaged results of the turbulent flow field.

At the right outflow boundary, x-independence of the profiles is assumed. Accordingly, $\partial\xi/\partial x = \partial v/\partial x = \partial\theta'/\partial x = 0$ and $\partial^2\psi/\partial z^2 = \xi$, i.e., $\partial w/\partial x = 0$.

The valley surface S (along which $z^* = 0$) lies a distance z_0 above the true physical surface. Along S, ψ is set to zero to ensure no perpendicular flow, a no-slip condition on velocity is imposed, and θ' is specified. Because of the explicitly modeled δ surface layer, however, these conditions must be indirectly applied through boundary conditions at the top of this layer. Expressions resulting from the integration of flux-profile relationships through the surface layer are used to specify ψ, ξ, v, and θ' at $z^* = \delta$ (Carlson, 1982). The special treatment given the turbulence model over sloping terrain is discussed in Carlson and Foster (1985).

c. *Nondimensionalization*

Let the valley depth H be chosen as the characteristic length scale in the present problem, $U_g = (u_g^2 + v_g^2)^{1/2}$ be the characteristic velocity scale, and $\Delta\theta$, the characteristic temperature scale, where $\Delta\theta$ represents the difference (taken as positive) in θ between $z = z_t$ and the surface S. Using these scales, one can nondimensionalize Eqs. (3)–(6). In the set of equations that results (Carlson and Foster, 1985), two nondimensional numbers appear, a bulk Richardson number (Ri_B) and the Rossby number (Ro), where

$$\mathrm{Ri}_B = -gH\Delta\theta/(U_g^2\theta_0), \tag{16}$$

$$\mathrm{Ro} = U_g/fH. \tag{17}$$

In the present problem the bulk Richardson number is especially important, since the baroclinic production term in the vorticity equation (4) becomes

$$\mathrm{Ri}_B\partial\theta'/\partial x,$$

where θ' and x are now in nondimensional units. In cases with Ri_B near zero (Carlson and Foster, 1985), this term is small, and dynamic interactions of the flow with the valley dominate; for flows with Ri_B of order one, the subject of this paper, the effect of buoyancy acting through this baroclinic vorticity-production term also becomes important.

The Rossby number, which indicates the relative importance of the inertia terms to the Coriolis terms, is very large in the present problem and thus suggests that Coriolis forces are largely unimportant in the valley

domain. Their main roles lie in determining the equilibrium inflow wind spiral and in allowing smooth transition to the Ekman spiral above z_t.

4. Numerical solution

The solution of the problem formulated in section 3 is determined numerically over a two-dimensional, uniform rectangular grid. The valley surface S is constrained to pass through the grid points and to have a slope of 0 or $\pm\Delta z/\Delta x$, where Δz and Δx are the nondimensional vertical and horizontal grid intervals, respectively; i.e., $\Delta z/\Delta x = \tan\alpha$.

Details of the numerical solution (3)–(6) are given in Carlson (1982) and Carlson and Foster (1985). A grid halving procedure is employed such that the final steady-state solution is over a grid with $\Delta z = 0.0625$. The alternating-direction implicit method (ADI) is used to advance ξ, v, and θ' over time to the steady-state solution; threefold iteration over each time step occurs. Successive over-relaxation (SOR) is used to solve for ψ at the end of each time step.

All derivatives in (3)–(6), as well as those in the boundary conditions, are represented by second-order (or higher) accurate finite differences. For the nonlinear advective terms, three-point backward differencing into the wind is used, leading to order $(\Delta x)^2$-accurate differencing and, hence, no development of artificial viscosity.

Truncation error studies (appendix D of Carlson, 1982; Carlson and Foster, 1985) show the percentage errors in the final fine-grid solutions to be generally below 2%. All calculations were performed in double-precision arithmetic on the Amdahl 470 V/6-II of The Ohio State University Instruction and Research Computer Center.

5. Numerical results

Table 1 presents the parameter values used in the three case studies as well as the resulting bulk Richardson and Rossby numbers. The only difference between the cases is the valley surface temperature. Case 1 is the base case, a valley with an isothermal surface. Case 2 represents a valley with a warmer windward slope and cooler leeward slope. In case 3 the situation is reversed, with the leeward slope being the warmer slope. The numerically large value for the Rossby number arises from the use of H as the length scale rather than the usual horizontal scale. In these studies $H = 125$ m, $W/H = 2.75$, $\alpha = 20°$, $z_0 = 0.1$ m, $\theta_0 = 300$ K, $X_r = 2W$, $\lambda = 100$ m, and $\delta^* = 2\delta$. Also, $k = 0.41$ and $f = 9.37 \times 10^{-5}$ s^{-1} ($\phi = 40°$).

TABLE 1. Parameter values for the three case studies.

Case	u_g (m s^{-1})	v_g (m s^{-1})	$\theta(z_t)$ (K)	$\theta(S)$ (K)	Ri_B	Ro
1	2	−1	298.6	300.0	−1.14	191
2	2	−1	298.6	302.0 Left slope 299.5 Right slope 300.0 Elsewhere	−2.77 −0.735 −1.14	191
3	2	−1	298.6	299.5 Left slope 302.0 Right slope 300.0 Elsewhere	−0.735 −2.77 −1.14	191

TABLE 2. Comparisons of eddy momentum exchange coefficients K_m from present model with those modeled and observed in Hanna (1968).

Elevation above surface (m)	K_m (m^2/s) Present model	Hanna's model	Range observed
	Over ridge at left boundary		
46	6.22	6.16	2–15
137	10.2	11.1	4–30
229	10.4	12.6	4–35
320	9.90	11.1	4–30
	Over center of valley		
46	5.17	5.26	2–15
137	20.0	10.5	4–30
229	25.2	11.1	4–30
320	23.5	7.29	3–20

Before we proceed with our numerical results, we would first like to comment on the magnitude of our eddy viscosity coefficients. As a check on the validity of our turbulence model, we compared our K_m values to those modeled and observed in Hanna (1968). Table 2 presents the K_m calculated by our turbulence model at heights of 46, 137, 229, and 320 m over the ridge at the left boundary and over the center of the valley (for case 1). Included for comparison with each of our K_m values are a K_m, calculated according to the Hanna model, and a range (about Hanna's K_m) of K_m values falling within a band encompassing all eddy viscosities observed at Cedar Hill (Fig. 5 of Hanna). The agreement between our K_m and Hanna's is excellent at all elevations at the left boundary; over the valley the agreement is excellent at 46 m but becomes progressively worse at higher elevations. Even there, however, all our values except that at 320 m fall within the band of observations. The discrepancies over the valley are not unexpected. First, the Cedar Hill observations were not taken within a valley. Second, the equation Hanna uses to calculate friction velocity is based on integrating a simplified form of the equation of motion, a form which certainly is not valid for nonhomogeneous valley flow. Note that over the valley the agreement of K_m is worse at higher elevations, where the influence of the valley side walls can be felt, but much better near the valley floor, where these topographic effects are minimal. With these considerations, therefore, our K_m values can be said to compare well with those of Hanna,

since only where flow is uniform (e.g., the left boundary) should the comparisons be made.

Figure 2 presents the perturbation potential temperature (θ') contours for the three cases. Note the strong heating off the left slope in case 2 and off the right slope in case 3. In the vicinity of the intense heating, the isotherms lie nearly parallel to the slope. An interesting difference between cases 2 and 3 can be seen, however. Because of the direction of the ambient airflow (left to right), a warmer left slope (Fig. 2b) is more effective in heating the valley than a warmer right slope (Fig. 2c). Note, for example, that the $\theta' = -0.60$ isotherm does not even enter the valley in case 2 (indeed, it slopes upward to the right), while in case 3 it first dips down into the valley before making its ascent.

Figure 3 presents the vorticity (ξ) contours for the three cases. Because of the $\mathrm{Ri}_B \partial\theta'/\partial x$ term in the nondimensionalized vorticity equation, isotherms which slope upward to the right will cause negative vorticity production in their vicinity. Those which slope downward to the right will contribute positively toward vorticity production. These effects can easily be seen in Fig. 3. Consider first the region over the left slope (Fig. 2). Except for the layer immediately above this slope, the case having the isotherms of greatest negative slope in this region is case 3, followed by case 1, and last, case 2. Accordingly, apart from the surface layer itself, one finds (Fig. 3) that case 3 has the largest region of significant vorticity (e.g., $\xi > 0.12$) over the left slope, followed by case 1, and last, case 2. Consider next the region over the right slope (Fig. 2). Here the isotherms having the greatest positive slope belong also to case 3, followed by cases 1 and 2. In Fig. 3 a large region of negative vorticity resides over the right slope in case 3, in accordance with the baroclinic production term. With cases 1 and 2 this region becomes one of small positive vorticity. The negative ξ values over the right ridge in case 2 arise from the upward-sloping isotherms upwind of this region.

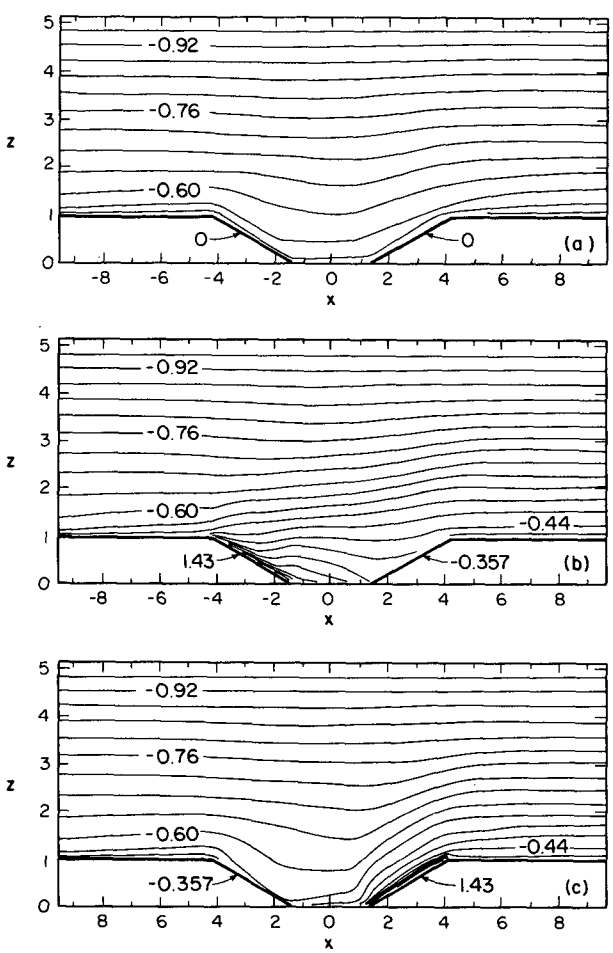

FIG. 2. Perturbation potential temperature (θ') contours for (a) case 1, (b) case 2, and (c) case 3. The contour interval is 0.04, with all isopleths within $\delta/2$ above the valley surface omitted; $\theta' = 0$ at all horizontal valley surfaces. All values are dimensionless, with θ' nondimensionalized by $\Delta\theta = 1.4$ K.

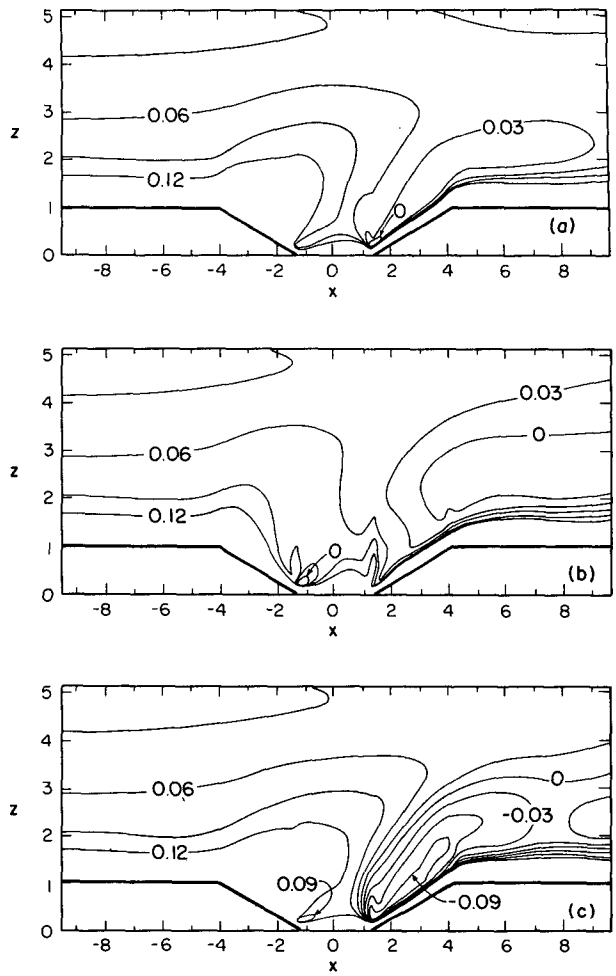

FIG. 3. Vorticity (ξ) contours for (a) case 1, (b) case 2, and (c) case 3. The contour interval is 0.03, with isopleths having ξ values exceeding 0.12 omitted. All values are nondimensional.

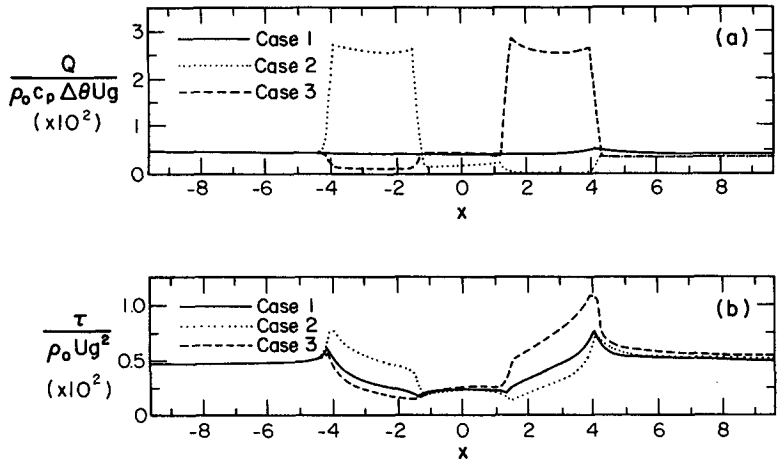

FIG. 4. Surface distributions of (a) heat flux normal to the surface (Q) and (b) shear stress (τ) for the three cases. All axis values are nondimensional; $\Delta\theta$ = 1.4 K in all cases.

The two surface parameters which correspond to θ' and ξ are the heat flux Q and shear stress τ. Figure 4 displays their distributions for the three cases. Note the large differences in Q between left and right slopes in cases 2 and 3. Also notice that on these slopes the magnitude of the surface stress is directly proportional to the amount of heat flux. Greater heating creates a higher degree of thermal turbulence, bringing down more ambient momentum from above and increasing the surface stress. Finally, note that while the heating rates off the respective slopes are nearly the same, case 3 has considerably larger τ values on the right slope than case 2 has on the left slope. This situation may also be explained through the baroclinic production term in Eq. (4). Above the right slope in case 3, the baroclinic creation of negative vorticity acts to decrease the magnitude of the wind speed shear, resulting in greater shear (and, hence, τ) immediately adjacent to the slope. In case 2, however, the baroclinic creation of positive vorticity above the left slope has the opposite effect, resulting in a lowering of τ. Even though the baroclinic contribution is subtractive over the left slope, case 2 still has, of all the cases, the highest surface stress values there due to the large amounts of ambient momentum brought down as a result of the intense turbulent mixing.

Figure 5 presents the vertical profiles of total wind speed for the three cases over the midpoints of the left and right valley slopes. In comparing one profile with another, a given profile will be said to be "fuller" if it has a greater slope (and, hence, greater τ) near the surface and a smaller slope farther above (e.g., at z = 1). Over the left slope case 2 has the fullest profile, followed by cases 1 and 3, in that order. This order corresponds with the ordering of the τ values at the left slope (Fig. 4b) as well as with the vorticity patterns farther above the surface (Fig. 3). Over the right slope case 3 has the fullest profile, followed by case 1, then case 2. This ordering, also, corresponds to the τ ordering in Fig. 4b and the vorticity patterns in Fig. 3. The profile of case 3, with a wind speed maximum a distance 0.3 above the surface, clearly is a manifestation of the baroclinic production of negative vorticity over the heated right slope.

Finally, Table 3 lists some numerical results from the case studies. Besides the τ and Q parameters already

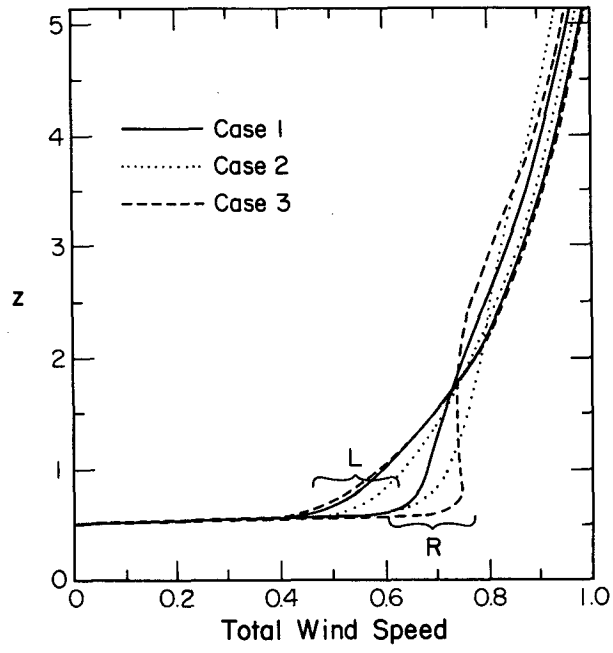

FIG. 5. Vertical profiles of total wind speed at two surface locations for the three cases. The L denotes those profiles over the midpoint of the left valley slope and R, those over the midpoint of the right slope. All values are nondimensional.

TABLE 3. Some numerical results from the three case studies. The term β_1 denotes the surface layer wind direction at the upper left corner of the valley; β_2, that at the lower left corner; β_3, that at the lower right corner; β_4, that at the upper right corner; τ, the surface shear stress; and Q, the heat flux normal to the surface. At the left inflow boundary, $\beta = 282.2°$, $\tau = 0.029$ N m^{-2}, and $Q = 18.6$ W m^{-2}.

Case	β_1 (deg)	β_2 (deg)	$\beta_2 - \beta_1$ (deg)	β_3 (deg)	β_4 (deg)	$\beta_4 - \beta_3$ (deg)	τ_{max} (N m^{-2})	τ_{min} (N m^{-2})	Q_{max} (W m^{-2})	Q_{min} (W m^{-2})
1	280.2	294.3	14.1	289.0	278.7	−10.3	0.0478	0.0105	20.1	15.2
2	280.1	290.6	10.5	288.9	277.7	−11.2	0.0473	0.00875	106.0	0.249
3	280.1	294.5	14.4	286.8	278.2	−8.6	0.0683	0.00867	112.0	4.24

discussed, the table lists the surface layer wind directions at the four corners of the valley. In another paper (Carlson and Foster, 1985), channeling of flow by the valley is examined through four case studies, each having a valley surface of constant temperature. In the present paper, however, the effects of variable heating off a slope on the angle of the wind as it passes over that slope can be investigated. In Table 3, $\beta_2 - \beta_1$ gives the degrees of turning (clockwise sense) of the surface layer wind as it passes over the left slope. Note that the amount of turning is least (10.5°) in case 2, which has the greatest amount of heating off the left slope, and greatest (14.4°) in case 3, which has the least amount of heating off that slope. Greater heating leads to greater turbulent mixing, resulting in less channeling. The quantity $\beta_4 - \beta_3$ over the right slope follows the same pattern; that is, the amount of directional turning over a slope being inversely related to the heating off that slope.

6. Discussion

The three cases which have been presented have bulk Richardson numbers ranging from −0.735 to −2.77, i.e., of order one. We have asserted that thermal effects become important for Ri_B numbers of this order, in contrast to Ri_B numbers close to zero, where such effects are negligible. The purpose of this section is to explore in a semiquantitative manner the effects of slope heating as revealed in our numerical results, especially in Fig. 5.

We will use the vorticity equation (4) to aid us in our discussion. Because the solution is steady state, the term on the left-hand side of Eq. (4) represents the advection of vorticity. On the right-hand side, the first term depicts the baroclinic production of vorticity; the second term, vorticity generation from Coriolis effects; and the last four terms, turbulent diffusion of vorticity. In the course of the research, it was seen that the Coriolis term is of little consequence, being one to three orders of magnitude smaller than the other terms. Thus, three main processes determine the wind structure: advection, baroclinic production, and turbulent diffusion.

While vorticity advection is important in explaining the details of a *particular* wind speed profile, it is our contention that it is relatively unimportant in explaining relative *differences* between profiles in our three cases, and that baroclinic production and turbulent diffusion need only be used in such explanations. First, baroclinic production and turbulent diffusion are the only two processes in (4) which are directly influenced by surface heating (the first through $\partial\theta'/\partial x$, the second through enhanced K_m values). Since surface heating is the only variable changed from case to case, it seems reasonable that these two processes should have the greater effects. Second, an examination of the streamline plots (ψ) in cases 1–3 (Carlson, 1982) shows the ψ structure to be nearly identical in all three cases, whereas vorticity (Fig. 3) and temperature (Fig. 2) plots are vastly different among the cases. Now vorticity advection is reflected in the ψ plots (through first and second derivatives); baroclinic production, in the θ plots (through horizontal gradients); and turbulent diffusion, in the ξ plots (through various derivatives). Accordingly, the latter two processes must be more instrumental in causing differences among the three cases than is advection. Third, a preliminary study showed *differences* in advection between cases over the left slope to be typically two orders of magnitude smaller than differences in baroclinic production and turbulent diffusion; over the right slope, the advection differences are typically one order of magnitude smaller. Lastly, as will be seen, using only the two processes of baroclinic production and turbulent diffusion produces a more than adequate explanation of the results and serves as an a posteriori argument.

We now take a look at these two processes in the three cases presented. Table 4 presents values of vorticity ξ, K_m (a measure of turbulent diffusion), and $\partial\theta/\partial x$ (a measure of baroclinic production) at various elevations above the midpoints of the left and right slopes.

First, one sees in Fig. 5 that over the right slope the profiles are fuller and of greater speed than their corresponding ones on the left. How might this observation be explained? Consider first the temperature plots in Fig. 2 (also refer to Table 4). Over the right slope, surface heating and subsequent diffusion result in isotherms which slope upward to the right ($\partial\theta/\partial x > 0$). This temperature structure generates negative vorticity through the baroclinic production term and acts to decrease the values of vorticity over the right slope. Over the left slope the surface heating results in isotherms which slope downward to the right ($\partial\theta/\partial x < 0$), except farther above the slope in case 2 where $\partial\theta/\partial x$ is slightly

TABLE 4. Values of vorticity (ξ), eddy viscosity (K_m), and horizontal temperature gradient ($\partial\theta/\partial x$) at various elevations above the midpoints of the left and right valley slopes.

Elevation above slope (m)	Case 1			Case 2			Case 3		
	ξ (10^{-3} s^{-2})	K_m (m^2 s^{-1})	$\partial\theta/\partial x$ (10^{-4} K m^{-1})	ξ (10^{-3} s^{-2})	K_m (m^2 s^{-1})	$\partial\theta/\partial x$ (10^{-4} K m^{-1})	ξ (10^{-3} s^{-2})	K_m (m^2 s^{-1})	$\partial\theta/\partial x$ (10^{-4} K m^{-1})
				Over left slope					
125.0	2.70	26.7	−1.39	2.09	28.6	0.697	2.91	22.2	−2.09
78.1	3.36	21.0	−1.86	2.65	23.5	0.697	3.84	16.8	−3.02
46.9	4.33	12.3	−2.56	3.53	15.1	0.0	5.12	9.45	−3.49
15.6	8.56	1.63	−14.6	8.96	2.73	−32.3	8.90	1.09	−8.84
				Over right slope					
125.0	0.415	22.0	1.39	0.347	11.7	1.63	−1.33	32.6	5.58
78.1	0.253	16.4	1.39	0.441	7.49	1.39	−1.67	26.3	6.28
46.9	0.302	8.44	2.79	1.12	3.39	2.09	−1.78	14.9	9.07
15.6	11.8	1.72	16.0	15.9	0.873	0.697	12.5	2.85	48.6

positive. This temperature structure generates positive vorticity and acts to increase the values of vorticity over the left slope. The baroclinicity within the valley thus helps to create greater vorticity values at heights above the left slope not immediately adjacent to the slope ($z > 15.6$ m in Table 4) and lower vorticity values at such heights above the right slope (see Fig. 3). Over the left slope, turbulent diffusion of air having higher vorticity thus results in wind speeds which decrease at greater rates as one approaches the slope from above. Hence, speeds are lower and the profiles less full (lower τ values) immediately over the left slope than over the right. Over the right slope, turbulent diffusion of air having lower vorticity results in higher surface wind speeds and fuller profiles (greater τ values). Note in Table 4 that ξ values are greater over the right slope at $z = 15.6$ m but smaller at $z > 15.6$ m as compared to the corresponding ξ values over the left slope. Also note in Fig. 5 how the intense generation of negative vorticity over the right slope in case 3 results in a ve-

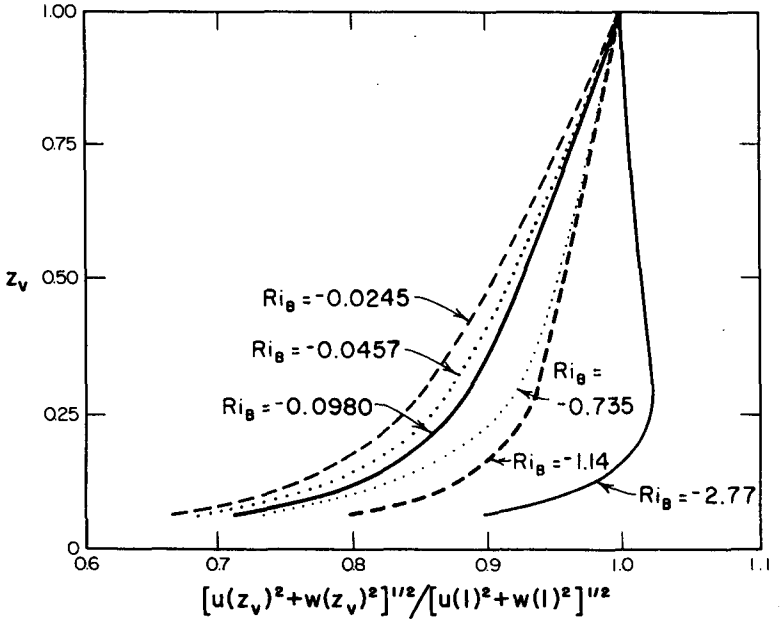

FIG. 6. Effect of bulk Richardson number on the shape of the normalized wind speed profile over the midpoint of the right valley slope. Variable z_v denotes the nondimensional height above the slope. The leftmost three profiles are taken from case studies described in Carlson (1982).

locity overshoot, similar to the shape of an upslope wind profile except for the eventual increase of speed with height to the value of the ambient wind.

Second, note in Fig. 5 that over a given slope the fullest wind speed profile (and greatest surface speeds) occurs in that case having the greatest surface heat flux (case 2 for the left slope and case 3 for the right). Consider first the left slope. Note in Table 4 how the eddy viscosities are directly related to the surface heat flux, with case 2 having the greatest K_m values, followed by case 1 and then case 3. Case 2 also has the lowest vorticities at intermediate heights above the left slope (note the slightly positive $\partial\theta/\partial x$ values). The fact that case 2 has the fullest profile over the left slope is clearly due to a combined effort whereby air having the lowest vorticity (due to baroclinic production) is mixed to the greatest degree. The profiles over the right slope may be explained in the same manner. Note how case 3, which has the fullest profile, has the greatest K_m values and lowest ξ values above 15.6 m. Thus, increasing the magnitude of the bulk Richardson number serves to increase the fullness of the wind speed profile above a given slope. Figure 6 shows this effect above the right slope through the addition of three cases taken from Carlson (1982) with Ri_B of smaller magnitudes.

Third, Fig. 5 shows that the wind speed separation between left and right profiles is greatest (at heights close to the slopes) in case 3, followed by case 1 and, last, case 2. This observation can also be explained by the same two processes of baroclinic production and turbulent diffusion. Consider the base case, case 1, which has both slopes at the same temperature. As heating is increased off the right slope and decreased off the left (case 3), these two processes will tend to increase the surface speeds off the right slope while decreasing them off the left (see prior explanations). Hence, the separation should be greater than in case 1. Starting with the base case again, as heating is now increased off the left slope and decreased off the right (case 2), surface speeds off the left slope will increase while decreasing on the right. The separation in this case is now less than in case 1. In Carlson (1982) it is seen that as the bulk Richardson number decreases in magnitude ($\mathrm{Ri}_B \rightarrow 0^-$), left and right wind speed profiles become more and more similar in shape until, under neutral conditions ($\mathrm{Ri}_B = 0$), they are nearly identical.

In all of our three cases, the flow over the left slope is downslope, in the same general direction as the ambient momentum further above. The absence of an upslope wind over windward valley slopes during conditions of unstable stratification and ambient wind has been confirmed observationally and numerically in other studies. The observational evidence has already been presented in the Introduction. In a numerical model Banta (1983) demonstrated the same phenomena—the development of easterly upslope flow after sunrise and the late morning surfacing of the well-mixed westerlies. Yamada (1980), in his numerical model, simulated ambient geostrophic flow of 2 m s^{-1} over a three-dimensional Gaussian valley. He too found upslope flow over the windward slopes to be a transient phenomenon, with such flows vanishing due to turbulent mixing by early afternoon. Such is the situation modeled in the present paper—a well-mixed, unstably stratified atmosphere typical of a sunny midafternoon.

Finally, it should be remarked that during evening conditions, surface cooling of the slopes will be more conducive to the formation of downslope winds over both slopes. The effect of surface cooling on turbulent mixing is now to decrease it, effectively decoupling the thermally driven surface flows from the ambient momentum above. Hence, downslope flow over the leeward slope should be much more likely than its counterpart in the daytime case (upslope flow over the windward slope).

7. Conclusions

A two-dimensional numerical model has been utilized to investigate steady state turbulent atmospheric flow over a valley under unstable thermal stratifications. Such situations are typical of midafternoon conditions on sunny days. The present paper examines flows at bulk Richardson numbers of order one and, as such, presents a contrast to Carlson and Foster (1985), wherein flows having bulk Richardson numbers near zero are investigated.

The case studies presented in this paper pertain, as mentioned, to flows having Ri_B of order one, i.e., to flows where the thermal effects of topography are of the same scale as the dynamic effects. The three cases examined differ only in the distribution of temperature at the valley surface. Some of the more salient conclusions from these case studies are as follows:

1) Surface heating affects the vorticity distribution directly through two processes: baroclinic production and turbulent diffusion.

2) Increased heating off a given slope (Ri_B increasingly negative) results in a fuller wind speed profile and a greater surface shear stress. It also decreases the amount of directional deflection the wind experiences as it moves over the slope.

3) Over the windward slope, baroclinic vorticity production is greater in value (generally positive) than over the leeward slope, and results in wind speed profiles that are lower in speed and less full than those over the right slope. Flow is always downslope.

4) Over the leeward slope, baroclinic vorticity production is negative, resulting in wind speed profiles of greater speed and fullness as compared to those over the windward slope. A profile having a velocity overshoot exists for the case having the largest (in magnitude) bulk Richardson number over the leeward slope.

Acknowledgments. The authors extend thanks to Professors O. R. Burggraf and A. T. Conlisk for their

interest and contributions during this research. Numerical calculations were performed at The Ohio State University Instruction and Research Computer Center. The preparation of this paper was supported in part by a grant from the Ohio Air Quality Development Authority (OSU Project Number 529629).

REFERENCES

Banta, R. M., 1981: The development of the heated boundary layer and associated flow systems in South Park, Colorado. *Preprints, Second Conference on Mountain Meteorology,* Steamboat Springs, Amer. Meteor. Soc., 283–288.

——, 1983: Numerical model simulations of the daytime development of flow over a heated ridge. *Extended Abstracts, Sixth Symposium on Turbulence and Diffusion,* Boston, Amer. Meteor. Soc., 169–172.

Bell, R. C., and R. O. R. Y. Thompson, 1980: Valley ventilation by cross winds. *J. Fluid Mech.,* **96,** 757–767.

Blackadar, A. K., 1962: The vertical distribution of wind and turbulent exchange in a neutral atmosphere. *J. Geophys. Res.,* **67,** 3095–3102.

Busch, N. E., 1973: On the mechanics of atmospheric turbulence. *Workshop on Micrometeorology,* D. A. Haugen, Ed., Boston, Amer. Meteor. Soc., 1–65.

Businger, J. A., 1973: Turbulent transfer in the atmospheric surface layer. *Workshop on Micrometeorology,* D. A. Haugen, Ed., Boston, Amer. Meteor. Soc., 67–100.

Carlson, J. D., 1982: Numerical calculation of steady-state turbulent atmospheric flows over a valley under neutral and unstable thermal stratifications. Ph.D. dissertation, Atmospheric Sciences Program, The Ohio State University, Columbus, Ohio, 320 pp.

——, and M. R. Foster, 1985: Numerical study of some neutrally and unstably stratified boundary-layer flows over a valley at small Richardson number. *Tellus* (in press).

Defant, F., 1951: Local winds. *Compendium of Meteorology,* T. F. Malone, Ed., Boston, Amer. Meteor. Soc., 655–672.

Dyer, A. J., and B. B. Hicks, 1970: Flux-gradient relationships in the constant flux layer. *Quart. J. Roy. Meteor. Soc.,* **96,** 715–721.

Hanna, S., 1968: A method of estimating vertical eddy transport in the planetary boundary-layer using characteristics of the vertical velocity spectrum. *J. Atmos. Sci.,* **25,** 1026–1033.

Hewson, E. W., and G. C. Gill, 1944: Meteorological investigations in Columbia River Valley near Trail, B.C. *Bur. of Mines Bull.,* **453,** 23–228.

Kao, S. K., and C. M. Liu, 1981: An analytical solution for three-dimensional stationary flows in the planetary boundary layer over mountain-valleys of infinite extent. *Extended Abstracts, Fifth Symp. on Turbulence, Diffusion, and Air Pollution,* Atlanta, Amer. Meteor. Soc., 212–215.

Lanham, L., 1980: Wintertime dispersion process in the Lake Tahoe basin. *Proc., Second Joint Conf. on Appl. of Air Pollution Meteorology,* New Orleans, Amer. Meteor. Soc., 520–525.

Tang, W., 1976: Theoretical study of cross-valley wind circulation. *Arch. Meteorol. Geophys. Bioklim.,* **A25,** 1–18.

Taylor, P. A., 1977a: Some numerical studies of surface boundary-layer flow above gentle topography. *Bound.-Layer Meteor.,* **11,** 439–465.

——, 1977b: Numerical studies of neutrally stratified planetary boundary-layer flow above gentle topography. *Bound.-Layer Meteor.,* **12,** 37–60.

Whiteman, C. D., 1982: Breakup of temperature inversions in deep mountain valleys: Part I. Observations. *J. Appl. Meteor.,* **21,** 270–289.

Yamada, T., 1980: Air circulations over a Gaussian-shaped valley. *Proc., Second Joint Conf. on Appl. of Air Pollution Meteorology,* New Orleans, Amer. Meteor. Soc., 505–509.

Yamamoto, G., N. Yasuda and A. Shimanuki, 1968: Effect of the thermal stratification on the Ekman layer. *J. Meteor. Soc. Japan,* **46,** 442–454.

Zilitinkevich, S., D. Laikhtman and A. S. Monin, 1967: Dynamics of the atmospheric boundary layer. *Isv., Atmos. Oceanic Phys.,* **3,** 297–333.